

REPORT DOCUMENTATION PAGE			Form Approved OMB NO. 0704-0188		
<p>The public reporting burden for this collection of information is estimated to average 1 hour per response, including the time for reviewing instructions, searching existing data sources, gathering and maintaining the data needed, and completing and reviewing the collection of information. Send comments regarding this burden estimate or any other aspect of this collection of information, including suggestions for reducing this burden, to Washington Headquarters Services, Directorate for Information Operations and Reports, 1215 Jefferson Davis Highway, Suite 1204, Arlington VA, 22202-4302. Respondents should be aware that notwithstanding any other provision of law, no person shall be subject to any penalty for failing to comply with a collection of information if it does not display a currently valid OMB control number. PLEASE DO NOT RETURN YOUR FORM TO THE ABOVE ADDRESS.</p>					
1. REPORT DATE (DD-MM-YYYY) 28-08-2015		2. REPORT TYPE Final Report		3. DATES COVERED (From - To) 1-Sep-2014 - 31-May-2015	
4. TITLE AND SUBTITLE Final Report: 4.3 Electronic Sensing - Depleted Nanocrystal-Oxide Heterojunctions for High-Sensitivity Infrared Detection			5a. CONTRACT NUMBER W911NF-14-1-0292		
			5b. GRANT NUMBER		
			5c. PROGRAM ELEMENT NUMBER 611102		
6. AUTHORS Xian-An Cao			5d. PROJECT NUMBER		
			5e. TASK NUMBER		
			5f. WORK UNIT NUMBER		
7. PERFORMING ORGANIZATION NAMES AND ADDRESSES West Virginia University Research Corporat 886 Chestnut Ridge Road P.O. Box 6845 Morgantown, WV 26506 -6845			8. PERFORMING ORGANIZATION REPORT NUMBER		
9. SPONSORING/MONITORING AGENCY NAME(S) AND ADDRESS (ES) U.S. Army Research Office P.O. Box 12211 Research Triangle Park, NC 27709-2211			10. SPONSOR/MONITOR'S ACRONYM(S) ARO		
			11. SPONSOR/MONITOR'S REPORT NUMBER(S) 65456-EL-II.2		
12. DISTRIBUTION AVAILABILITY STATEMENT Approved for Public Release; Distribution Unlimited					
13. SUPPLEMENTARY NOTES The views, opinions and/or findings contained in this report are those of the author(s) and should not be construed as an official Department of the Army position, policy or decision, unless so designated by other documentation.					
14. ABSTRACT The goal of this project is to explore a new IR photodetector architecture based on a depleted ZnO/PbS QD heterojunction. Colloidal PbS QDs with the first excitonic absorption peak from 850-1050 nm were synthesized, and ZnO thin films were prepared by two different methods: thermal evaporation and solution processing. Devices with an optimized ZnO/PhS QD structure showed ultralow dark current, fast response, and a photocurrent on/off ratio greater than 10000. A comparative study of ZnO or PhS QD single-layer structures proved that the optical response arises from charge separation at a depleted junction forming between ZnO and PbS QDs. However, near					
15. SUBJECT TERMS infrared, photodetector, quantum dot					
16. SECURITY CLASSIFICATION OF:		17. LIMITATION OF ABSTRACT UU	15. NUMBER OF PAGES	19a. NAME OF RESPONSIBLE PERSON Xian-An Cao	
a. REPORT UU	b. ABSTRACT UU			c. THIS PAGE UU	19b. TELEPHONE NUMBER 304-293-9684

Report Title

Final Report: 4.3 Electronic Sensing - Depleted Nanocrystal-Oxide Heterojunctions for High-Sensitivity Infrared Detection

ABSTRACT

The goal of this project is to explore a new IR photodetector architecture based on a depleted ZnO/PbS QD heterojunction. Colloidal PbS QDs with the first excitonic absorption peak from 850-1050 nm were synthesized, and ZnO thin films were prepared by two different methods: thermal evaporation and solution processing. Devices with an optimized ZnO/PhS QD structure showed ultralow dark current, fast response, and a photocurrent on/off ratio greater than 10000. A comparative study of ZnO or PhS QD single-layer structures proved that the optical response arises from charge separation at a depleted junction forming between ZnO and PbS QDs. However, poor charge transport through the solution-processed ZnO and QD layers limits the photoconductive gain and quantum efficiency of devices.

Enter List of papers submitted or published that acknowledge ARO support from the start of the project to the date of this printing. List the papers, including journal references, in the following categories:

(a) Papers published in peer-reviewed journals (N/A for none)

<u>Received</u>	<u>Paper</u>
-----------------	--------------

TOTAL:

Number of Papers published in peer-reviewed journals:

(b) Papers published in non-peer-reviewed journals (N/A for none)

<u>Received</u>	<u>Paper</u>
-----------------	--------------

TOTAL:

Number of Papers published in non peer-reviewed journals:

(c) Presentations

X. A. Cao, Y. Lu, and L. Y. Liu, "Tuning luminescence from nanocrystal heterostructures by bandgap and strain engineering," The 7th International Photonics and OptoElectronics Meeting, Wuhan, China June18-21, 2014 (invited talk).

Number of Presentations: 1.00

Non Peer-Reviewed Conference Proceeding publications (other than abstracts):

Received Paper

TOTAL:

Number of Non Peer-Reviewed Conference Proceeding publications (other than abstracts):

Peer-Reviewed Conference Proceeding publications (other than abstracts):

Received Paper

TOTAL:

Number of Peer-Reviewed Conference Proceeding publications (other than abstracts):

(d) Manuscripts

Received Paper

08/28/2015 1.00 Xian-An Cao, Yifei Lu. Luminescence enhancement of nanocrystal quantum wells by bandgap and strain engineering, Journal of Nanophotonics (05 2015)

TOTAL: 1

Number of Manuscripts:

Books

Received Book

TOTAL:

Received Book Chapter

TOTAL:

Patents Submitted

None

Patents Awarded

None

Awards

None

Graduate Students

<u>NAME</u>	<u>PERCENT SUPPORTED</u>	<u>Discipline</u>
Yifei Lu	0.20	
Xiaomeng Li	0.25	
Renyan Yang	0.25	
FTE Equivalent:	0.70	
Total Number:	3	

Names of Post Doctorates

<u>NAME</u>	<u>PERCENT SUPPORTED</u>
FTE Equivalent:	
Total Number:	

Names of Faculty Supported

<u>NAME</u>	<u>PERCENT SUPPORTED</u>	National Academy Member
Xian-An Cao	0.05	
FTE Equivalent:	0.05	
Total Number:	1	

Names of Under Graduate students supported

<u>NAME</u>	<u>PERCENT SUPPORTED</u>
FTE Equivalent:	
Total Number:	

Student Metrics

This section only applies to graduating undergraduates supported by this agreement in this reporting period

The number of undergraduates funded by this agreement who graduated during this period: 0.00

The number of undergraduates funded by this agreement who graduated during this period with a degree in science, mathematics, engineering, or technology fields:..... 0.00

The number of undergraduates funded by your agreement who graduated during this period and will continue to pursue a graduate or Ph.D. degree in science, mathematics, engineering, or technology fields:..... 0.00

Number of graduating undergraduates who achieved a 3.5 GPA to 4.0 (4.0 max scale):..... 0.00

Number of graduating undergraduates funded by a DoD funded Center of Excellence grant for Education, Research and Engineering:..... 0.00

The number of undergraduates funded by your agreement who graduated during this period and intend to work for the Department of Defense 0.00

The number of undergraduates funded by your agreement who graduated during this period and will receive scholarships or fellowships for further studies in science, mathematics, engineering or technology fields:..... 0.00

Names of Personnel receiving masters degrees

<u>NAME</u>	
Yifei Lu	
Total Number:	1

Names of personnel receiving PHDs

<u>NAME</u>
Total Number:

Names of other research staff

NAME

PERCENT SUPPORTED

FTE Equivalent:

Total Number:

Sub Contractors (DD882)

Inventions (DD882)

Scientific Progress

Photoconductive response of a depleted ZnO/PbS QD heterojunction was experimentally confirmed. This work raises the prospect of developing a new type of low-cost, light-weight, and highly sensitive IR photodetectors based on the depleted ZnO/PbS QD heterojunction architecture.

Technology Transfer

None

Final Progress Report

Project title: Depleted Nanocrystal-Oxide Heterojunctions for High- Sensitivity Infrared
Detection

Contract No. W911NF-14-1-0292 (STIR)

Project Period: 09/01/2014-05/31/2015

PI: Xian-An (Andrew) Cao

Associate Professor

Department of Computer Science and Electrical Engineering
West Virginia University

(1) Foreword (optional)

The goal of this project is to explore a new IR photodetector architecture based on a depleted PbS QDs/ZnO heterojunction. During the 9-month period, efforts were made to optimize the preparation of two critical components: ZnO thin film and PbS QDs, and characterize the photocurrent response of the ZnO/PbS QDs bilayer structure. The proposed photodetection mechanism was confirmed, and a working device was demonstrated, but its responsivity and quantum efficiency were limited by slow charge transport in the solution-processed ZnO and QD layers.

(2) Table of Contents

List of Appendixes and Illustrations	2
Statement of the problem studied	2
Summary of the most important results	3
Bibliography	5
Appendix A: Form 298	6
Appendix B: Technical Report	9
Appendix C. DD Form 882	14
Appendix D. JNP paper	15

(3) List of Appendixes, Illustrations and Tables

Illustrations:

Figure 1. Current evolution in devices biased at 5 V measured in dark and under light.

Figure 2. Photocurrent response of a device biased at 5 V during a cycling test.

Figure 3. Spectral photocurrent response of a device biased at 5 V. The inset shows the absorption spectra of ITO/glass and ZnO/ITO/glass structures.

Appendixes:

A. Form 298

B. Technical Report

C. DD Form 882

D. Paper to be published in JNP

(4) Statement of the problem studied

Even though silicon photodiodes dominate in the market of imaging applications at visible and near-infrared wavelengths, they cannot operate for most of the infrared spectrum, beyond 1.1 μm . IR photodetectors based on many other materials show high noise levels or are difficult to fabricate using standard microfabrication techniques,^{1,2} and thus are either insensitive or very expensive. Therefore, there is a strong need to find new materials and device schemes that enable high-sensitivity detection of IR light at a reasonable cost.

Monodispersed colloidal nanocrystal quantum dots (QDs) synthesized and processed by low-cost solution methods has offered a new class of materials with desirable properties for optoelectronic applications including photodetection.²⁻⁴ However, the development of QD-based photodetection has not received much attention until recently. High-performance QD-based IR imaging and photodetection devices which have excellent overall performance and can be easily integrated with Si electronics have yet to be developed.

This project aims to fabricate a depleted PbS QDs/ZnO heterojunction and evaluate its applicability for IR photodetection. Through a study of the photoconductive behaviors and probing the mechanism of photocurrent generation, we hope to validate the design and proof of concept of a new effective IR photodetection architecture.

(5) Summary of the most important results

The ZnO/PbS QD heterojunction was fabricated on glass substrates with pre-patterned ITO (sheet resistance $\sim 15 \Omega/\text{sq}$). Both the ZnO and QD layers were formed by spin coating, from a sol-gel ZnO solution and a QD/hexane solution, respectively. Al contacts of 100-500 μm in diameter were deposited through a shadow mask as the cathode. Under illumination by a 70 W/m^2 incandescence white lamp, the device exhibited strong photoconductive response. Fig. 1 shows the evolution dark current and photocurrent under a constant voltage of 5 V. The dark current starts from 1×10^{-9} A and quickly drops to 10^{-11} A range. Upon illumination, the photocurrent increases gradually and peaks at $\sim 1.5 \times 10^{-8}$ A after 40 s. This value is about three orders of magnitude higher than the dark current. The initial increase is likely due to the fact that charge trapping at the QD/Al interface lowers the barrier and enhances hole collection at the anode.⁵ At the peak, the responsivity of the device is estimated to be only ~ 0.02 A/W. As seen, the photocurrent exhibits a gradual decay after reaching the peak value, which can be attributed to degradation of the unencapsulated PbS QDs which are prone to oxidation.

We also prepared structures consisting of a single QD layer or a single ZnO layer, but did not observe any photoconductive response. These comparisons confirm that the photocurrent observed above originates from the ZnO/QD heterojunction. Another interesting finding is that the dark current, on the order of 10^{-11} A, is considerably lower compared with that in a single ZnO layer (10^{-8} A). The dark current was further reduced using a thinner ZnO prepared from a diluted solution, down to 10^{-12} A, which is close to the limit of the testing system. These results indicate that the ZnO layer was partially depleted. Based on these observations, we conclude that a depleted junction indeed forms at the ZnO/QD interface, where the built-in electric field enables efficient separation of photogenerated carriers.

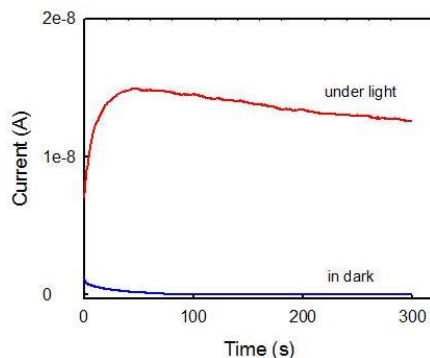


Fig. 1 current evolution in devices biased at 5 V measured in dark and under light.

Figure 2 shows the photocurrent response recorded at a fixed bias of 5 V to on/off illumination cycles. The photocurrent on/off ratio is greater than 10^3 , and the abrupt changes during the cycling test reflect rapid responses of the device to light. The speed is likely limited by the switching of the incandescent lamp. The highest on/off ratio $\sim 2 \times 10^4$, was obtained from devices with a thinner ZnO layer. The data in Fig. 6 demonstrates very good repeatability, but gradual degradation of the device is also seen, as indicated by a slow decay of the peak photocurrent.

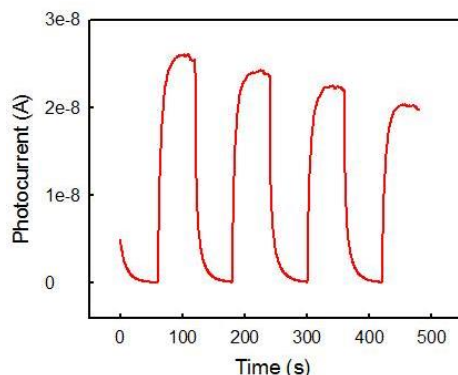


Fig. 2 Photocurrent response of a device biased at 5 V during a cycling test.

The spectral response of photocurrent measured using a 150 W Xenon lamp is shown in Fig. 3. The photocurrent is on the order of 1×10^{-7} A across the spectrum except a peak around 400 nm. The peak correlates well with strong light absorption by ZnO between 300 - 400 nm, as seen from the inset of Fig. 3. Therefore, there are two possible factors accounting for the enhanced photocurrent between 300-400 nm: (i) the ZnO layer absorbs light more efficiently than PbS QDs; (ii) A wider depletion region exists at the ZnO side compared to that on the PbS side, enabling dissociation of photogenerated excitons over a broader region. However, even at the peak wavelength, the external quantum efficiency (EQE) of this device is only $\sim 0.3\%$. It is believed that the performance (QE and responsivity) of the device is mainly limited by slow charge transport through the ZnO and QD layers. In the QD solid, dot-to-dot charge transfer is hampered by the bulky organic ligands.⁶ In the ZnO layer, the electron mobility has been found to be in the 10^{-3} - 10^{-4} $\text{cm}^2\text{V/s}$ range,⁷ comparable with that in a typical PbS QD solid.⁶ Therefore, the charge transit times in both ZnO and QD layers are longer than the carrier recombination lifetime. In other words, recombination dominates and there is no swept-out of electrons and holes, giving rise to a small photoconductive gain < 1 . In the meantime, the photocurrent may also be limited by inefficient charge collection at the electrodes which were not optimized in this work.

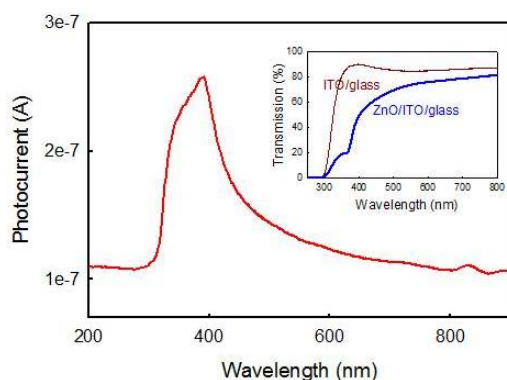


Fig. 3 Spectral photocurrent response of a device biased at 5 V. The inset shows the absorption spectra of ITO/glass and ZnO/ITO/glass structures.

In summary, a ZnO/PbS QD heterojunction was fabricated through solution processing, and its photoconductive behaviors were investigated. The devices exhibited a dark current as low as 10^{-12} A at a 5 V bias. Under illumination by a 70 W/m^2 incandescent lamp, a photocurrent on/off ratio greater than 10^4 was obtained. A comparative study of single-layer structures confirms that the photocurrent response originates from exciton dissociation at the heterojunction. The device, however, exhibited low responsivity of 0.02 A/W and peak quantum efficiency of 0.3%, mainly due to poor charge transport through the solution-processed ZnO and QD layers.^{7,8} Further work for performance enhancement will focus on: (i) contact optimization for more efficient charge collection; (ii) ligand exchange of the QDs for improved hole transport in the PbS QD solid;⁸ and (iii) preparation of high-quality ZnO films with a high electron mobility by other techniques such as sputtering deposition.

(6) Bibliography

1. S. Donati, "Photodetectors: Devices, Circuits and Applications," Prentice Hall, 1999.
2. D. V. Talapin, J. Lee, M. V. Kovalenko and E. V. Shevchenko, "Prospects of Colloidal Nanocrystals for Electronic and Optoelectronic Applications," *Chem. Rev.* 110, 389-458 (2010).
3. G. Konstantatos and E. H. Sargent, "Nanostructured materials for photon detection," *Nature Photon.* 5, 391-400 (2010).
4. G. Konstantatos and E. H. Sargent, "Colloidal quantum dot photodetectors," *Infrared Phys. Technol.* 54 (2011) 278–282.
5. Katz, G. Bahir, J. Salzman, *Appl. Phys. Lett.* 84, 4092 (2004).
6. Y. Sun, J. H. Seo, C. J. Takacs, J. Seifert, A. J. Heeger, *Adv. Mater.* 23 (14), 1679–1683, 2011.
7. J. Tang, K. Kemp, S. Hoogland, K. S. Jeong, H. Liu, L. Levina, M. Furukawa, X. Wang, R. Debnath, D. Cha, K. Chou, A. Fischer, A. Amassian, J. B. Asbury, and E. H. Sargent, *Nature Materials*, 10, 765-771 (2011).
8. Y. Q. Zhang and X. A. Cao, *Nanotechnology*, 23, 275702 (2012).

(7) Appendixes

A. Form 298

B. Technical Report

C. DD Form 882

REPORT DOCUMENTATION PAGE			<i>Form Approved</i> <i>OMB No. 0704-0188</i>		
Public reporting burden for this collection of information is estimated to average 1 hour per response, including the time for reviewing instructions, searching existing data sources, gathering and maintaining the data needed, and completing and reviewing this collection of information. Send comments regarding this burden estimate or any other aspect of this collection of information, including suggestions for reducing this burden to Department of Defense, Washington Headquarters Services, Directorate for Information Operations and Reports (0704-0188), 1215 Jefferson Davis Highway, Suite 1204, Arlington, VA 22202-4302. Respondents should be aware that notwithstanding any other provision of law, no person shall be subject to any penalty for failing to comply with a collection of information if it does not display a currently valid OMB control number. PLEASE DO NOT RETURN YOUR FORM TO THE ABOVE ADDRESS.					
1. REPORT DATE (DD-MM-YYYY) 08/20/2015		2. REPORT TYPE Final		3. DATES COVERED (From - To) 09/01/2014-05/31/2015	
4. TITLE AND SUBTITLE Depleted Nanocrystal-Oxide Heterojunctions for High-Sensitivity Infrared Detection			5a. CONTRACT NUMBER W911NF-14-1-0292		
			5b. GRANT NUMBER		
			5c. PROGRAM ELEMENT NUMBER		
6. AUTHOR(S) Xian-An (Andrew) Cao (The PI)			5d. PROJECT NUMBER 0010531957		
			5e. TASK NUMBER		
			5f. WORK UNIT NUMBER		
7. PERFORMING ORGANIZATION NAME(S) AND ADDRESS(ES) West Virginia University PO Box 6109 Morgantown, WV, 26506			8. PERFORMING ORGANIZATION REPORT NUMBER		
9. SPONSORING / MONITORING AGENCY NAME(S) AND ADDRESS(ES) U.S. Army Research Office Research Triangle Park, NC 27709-2211			10. SPONSOR/MONITOR'S ACRONYM(S) ARO		
			11. SPONSOR/MONITOR'S REPORT NUMBER(S)		
12. DISTRIBUTION / AVAILABILITY STATEMENT Approved for public release; distribution unlimited					
13. SUPPLEMENTARY NOTES					
14. ABSTRACT The goal of this project is to explore a new IR photodetector architecture based on a depleted ZnO/PbS QD heterojunction. Colloidal PbS QDs with the first excitonic absorption peak from 850-1050 nm were synthesized, and ZnO thin films were prepared by two different methods: thermal evaporation and solution processing. Devices with an optimized ZnO/PbS QD structure showed ultralow dark current, fast response, and a photocurrent on/off ratio greater than 10 ³ . A comparative study of ZnO or PbS QD single-layer structures proved that the optical response arises from charge separation at a depleted junction forming between ZnO and PbS QDs. However, poor charge transport through the solution-processed ZnO and QD layers limits the photoconductive gain and quantum efficiency of devices.					
15. SUBJECT TERMS infrared, photodetector, quantum dot					
16. SECURITY CLASSIFICATION OF:		17. LIMITATION OF ABSTRACT	18. NUMBER OF PAGES	19a. NAME OF RESPONSIBLE PERSON Dr. William Clark	

a. REPORT U	b. ABSTRACT U	c. THIS PAGE U	UU	3	19b. TELEPHONE NUMBER (include area code) (919) 549-4314
----------------	------------------	-------------------	----	---	---

Standard Form 298 (Rev. 8-98)
Prescribed by ANSI Std. Z39.18

(1) Submissions or publications under ARO sponsorship **during this reporting period**. List the title of each and give the total number for each of the following categories:

(a) Papers published in peer-reviewed journals

“Luminescence enhancement of nanocrystal quantum wells by bandgap and strain engineering” accepted for publication in Journal of Nanophotonics.

(b) Papers published in non-peer-reviewed journals

(c) Presentations

i. Presentations at meetings, but not published in Conference Proceedings

X. A. Cao, Y. Lu, and L. Y. Liu, “Tuning luminescence from nanocrystal heterostructures by bandgap and strain engineering,” The 7th International Photonics and OptoElectronics Meeting, Wuhan, China June 18-21, 2014 (invited talk).

ii. Non-Peer-Reviewed Conference Proceeding publications (other than abstracts)

X. A. Cao, Y. Lu, and L. Y. Liu, “Tuning luminescence from nanocrystal heterostructures by bandgap and strain engineering”

OSA Technical Digest (online) (Optical Society of America, 2014), paper OF3C.1 •doi:10.1364/OEDI.2014.OF3C.1

iii. Peer-Reviewed Conference Proceeding publications (other than abstracts)

(d) Manuscripts

(e) Books

(f) Honor and Awards

(g) Title of Patents Disclosed during the reporting period

(h) Patents Awarded during the reporting period

None

(2) Student/Supported Personnel Metrics **for this Reporting Period** (name, % supported, %Full Time Equivalent (FTE) support provided by this agreement, and total for each category):

(a) Graduate Students

1. Yifei Lu - 20% (one semester)

2. Xiaomeng Li - 25% (one semester)

3. Renyuan Yang – 25% (one semester)

(b) Post Doctorates

None

(c) Faculty

Xian-An Cao (PI) – 5% (0.5 month of summer pay)

(d) Undergraduate Students- 3 –

None

(e) Graduating Undergraduate Metrics (funded by this agreement and graduating during this reporting period):

i. Number who graduated during this period

none

ii. Number who graduated during this period with a degree in science, mathematics, engineering, or technology fields

none

iii. Number who graduated during this period and will continue to pursue a graduate or Ph.D. degree in science, mathematics, engineering, or technology fields

none

iv. Number who achieved a 3.5 GPA to 4.0 (4.0 max scale)

v. Number funded by a DoD funded Center of Excellence grant for Education, Research and Engineering

vi. Number who intend to work for the Department of Defense

vii. Number who will receive scholarships or fellowships for further studies in science, mathematics, engineering or technology fields

none

(f) Masters Degrees Awarded (Name of each, Total #)

Yifei Lu (Now an Application Engineer at Hermes-Microvision, Inc., CA)

(g) Ph.D.s Awarded (Name of each, Total #)

None

(h) Other Research staff (Name of each, FTE % Supported for each, Total % Supported)

None

(3) "Technology transfer" (any specific interactions or developments which would constitute technology transfer of the research results). Examples include patents, initiation of a start-up company based on research results, interactions with industry/Army R&D Laboratories or transfer of information which might impact the development of products.

None

(4) Scientific Progress and Accomplishments (description should include significant theoretical or experimental advances)

Photoconductive response of a depleted ZnO/PbS QD heterojunction was experimentally confirmed. This work raises the prospect of developing a new type of low-cost, light-weight, and highly sensitive IR photodetectors based on the depleted ZnO/PbS QD heterojunction architecture.

(5) "Copies of technical reports," which have **not** been previously submitted to the ARO, should be submitted concurrently with the Interim Progress Report. (See page 6 "Technical Reports" section for instructions.) However, do not delay submission while awaiting Reprints of publications.

A detailed technical report is attached.

Technical Report

1. Experimental Details

(a) Synthesis of PbS QDs

Colloidal PbS QDs capped with oleate ligands were synthesized using the conventional hot-injection method.¹ PbO and bis(trimethylsilyl) sulfide (TMS) were used as the precursors. The growth temperature was maintained at 100 °C and the growth time was varied from 30 sec to 30 mins. After extraction, the QDs were subjected to a multistep precipitation and redissolution process of purification to remove side products and unreacted precursors. As-synthesized QDs were then dispersed in hexane for optical measurements. The absorption spectra were measured using a Hitachi U-3900H double-beam UV-VIS spectrophotometer. However, fluorescence could not be obtained as the QD emission was beyond the wavelength range (300-800 nm) of our Hitachi F-7000 fluorescence spectrophotometer. As seen in Fig. 1, when the growth time was varied from 30 sec to 30 mins, the first excitonic absorption peak shifted from 850 to 1050 nm. During the first three months of the project period, the synthesis recipe (mainly the precursor concentrations and ratios) was optimized to obtain QDs with a strong excitonic absorption peak at 1050 nm.

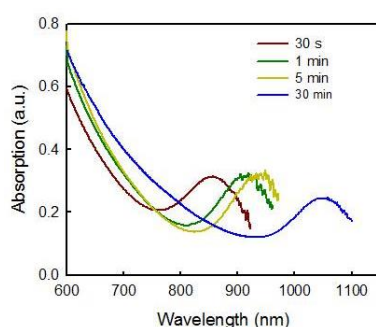


Fig. 1 Absorption spectra of PbS QDs with different growth times.

(b) Preparation of ZnO thin films

The initial effort was made to prepare ZnO thin films on ITO/glass by thermal evaporation of ZnO.² It has been found that the process is very hard to control. When the thickness was less than 20 nm, the film was not continuous due to its rough morphology and showed very high resistivity. For thicker films, the conductivity of the reduced ZnO was too high (even after annealing in air), making it unsuitable for photoconduction because the dark current and the associated noise would be too high.

A solution process was then developed to form more uniform ZnO films. Zn(Ac)₂ was dissolved in ethanolamine (NH₂CH₂CH₂OH) and 2-methoxyethanol (CH₃OCH₂CH₂OH), and stirred vigorously overnight to form a sol gel solution. ZnO thin films were prepared by spin coating at 4000 rpm for 1 min and annealing at different temperatures up to 400 °C for 10 min. To optimize the film thickness, spin coating was carried out from solutions with different concentrations. Fig. 2 shows the

I-V characteristics of ZnO thin film conductors measured between two Al contacts. As seen, the conductivity changes upon post-annealing as solvents are removed and the material is densified. For all the annealed films, the resistance values are greater than 30 M Ω , well suited for photoconductivity measurements.

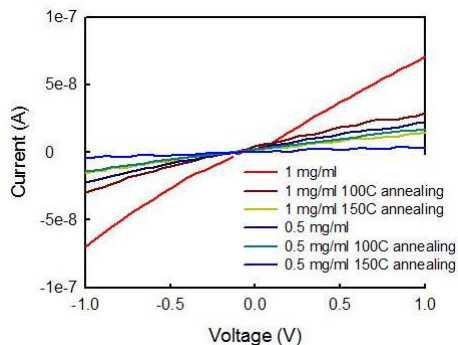


Fig. 2 I-V characteristics of solution-processed ZnO thin films.

(c) Fabrication of device structures

The photodetectors were fabricated on glass substrates with pre-patterned ITO (sheet resistance $\sim 15 \Omega/\text{sq}$). The substrates were cleaned with solvents and de-ionized water. They were then transferred to a N₂-filled glovebox where the ZnO and QD (20 mg/ml in hexane) layers were formed by spin-coating. Finally, the samples were transferred into a thermal evaporation system, where Al contacts of 100-500 μm in diameter were deposited through a shadow mask, acting as the cathode. A photograph of the completed devices is shown below.

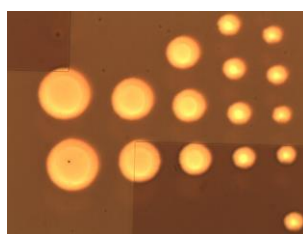


Fig. 3 Photography of completed photoconductive devices.

The electrical characteristics of the devices were measured using an Agilent 4156C semiconductor analyzer. Photocurrent responses were measured using an incandescence white lamp (70 W/m^2) under a microscope at a constant voltage of 5 V. Spectral responses of photocurrent in the devices were measured using a 150 W Xenon lamp source through a monochromator which was synchronized with an Agilent 4156C semiconductor analyzer.

2. Device Characterization Results and Discussion

Figure 4 shows the I-V characteristics of the photoconductor structure measured

between the ITO cathode and Al anode in dark and under illumination. The sharp increase in the current under light evidences the photoconductive response of the device. Note that no light is absorbed by ZnO since the white light spectrum cuts off at ~ 400 nm. Therefore, the photocurrent results from light absorption and carrier generation in the PbS QDs. We further prepared structures consisting of a QD layer only or a ZnO layer only, but did not observe any photoconductive response. The comparisons confirm that the photocurrent observed above originates from the ZnO/QD heterojunction. Another interesting finding is that the dark current, on the order of 10^{-11} A, is considerably lower compared with that in a single ZnO layer, indicating that the ZnO layer is partially depleted. Based on these observations, we may conclude that a depleted junction indeed forms at the ZnO/QD interface, enabling efficient separation of photogenerated carriers.

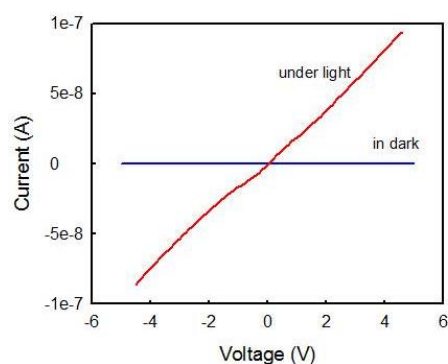


Fig. 4 I-V characteristics of a ZnO/PbS junction measured in dark and under a white incandescent light.

The current evolution under a constant voltage of 5 V was measured and plotted in Fig. 5. The dark current starts from 1×10^{-9} A and quickly drops to 10^{-11} A range. Upon illumination, the photocurrent increases gradually and peaks at $\sim 1.5 \times 10^{-8}$ A after 40 s. This value is about three orders of magnitude higher than the dark current. The initial increase is likely due to the fact that charge trapping at the QD/Al interface lowers the barrier and enhances hole collection at the anode.³ The result indicates that the photocurrent may be further improved by modifying the anode contact to the PbS QDs. At the peak, the responsivity of the device is estimated to be only ~ 0.02 A/W. As seen, the photocurrent exhibits a gradual decay after reaching the peak value, which can be attributed to degradation of the unencapsulated PbS QDs which are prone to oxidation.

Figure 6 shows the photocurrent response recorded at a fixed bias of 5 V to on/off illumination cycles. The photocurrent on/off ratio is greater than 10^3 , and the abrupt changes during the cycling test reflect rapid responses of the device to light. The speed is likely limited by the switching of the incandescent lamp. We further found that the dark current can be reduced using a thinner ZnO prepared from a diluted solution, down to 10^{-12} A, which is close to the limit of the testing system. The highest on/off ratio obtained from devices with a thin ZnO layer was 2×10^4 . The data in Fig. 6 demonstrates very good repeatability, but gradual degradation of the device

is also seen, as indicated by a slow decay of the peak photocurrent.

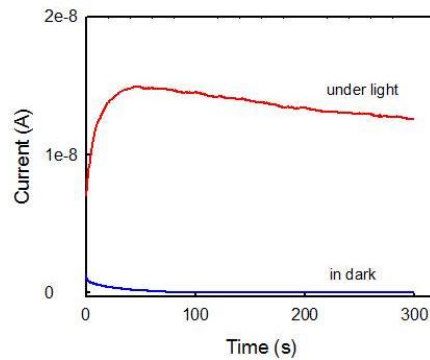


Fig. 5 Current evolution in devices biased at 5 V measured in dark and under light.

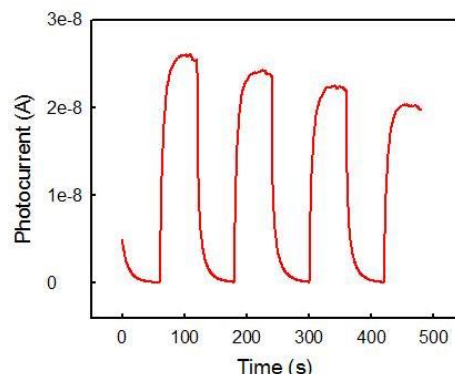


Fig. 6 Photocurrent response of a device biased at 5 V during a cycling test.

The spectral response of photocurrent measured using a 150 W Xenon lamp is shown in Fig. 7. The photocurrent is on the order of 1×10^{-7} A across the spectrum except a peak around 400 nm. The peak correlates well with strong light absorption by ZnO between 300 - 400 nm, as seen from the inset of Fig. 7. Therefore, there are two possible factors accounting for the enhanced photocurrent between 300-400 nm: (i) the ZnO layer absorbs light more efficiently than PbS QDs; (ii) A wider depletion region exists at the ZnO side compared to that on the PbS side, enabling dissociation of photogenerated excitons over a broader region. However, even at the peak wavelength, the external quantum efficiency (EQE) of this device is only $\sim 0.3\%$. It is believed that the performance (QE and responsivity) of the device is mainly limited by slow charge transport through the ZnO and QD layers. In the QD solid, dot-to-dot charge transfer is hampered by the bulky organic ligands.⁴ In the ZnO layer, the electron mobility has been found to be in the 10^{-3} - 10^{-4} $\text{cm}^2\text{V/s}$ range,⁵ comparable with that in a typical PbS QD solid.⁶ Therefore, the charge transit times in both ZnO and QD layers are longer than the carrier recombination lifetime. In other words, recombination dominates and there is no swept-out of electrons and holes, giving rise to a small photoconductive gain < 1 . In the meantime, the photocurrent may also be limited by inefficient charge collection at the electrodes which were not optimized in this work. Further work for performance enhancement should focus on: (i) contact

optimization for more efficient charge collection; (ii) ligand exchange of the QDs for improved hole transport in the PbS QD solid; and (iii) preparation of high-quality ZnO films with a high electron mobility by other techniques such as sputtering.

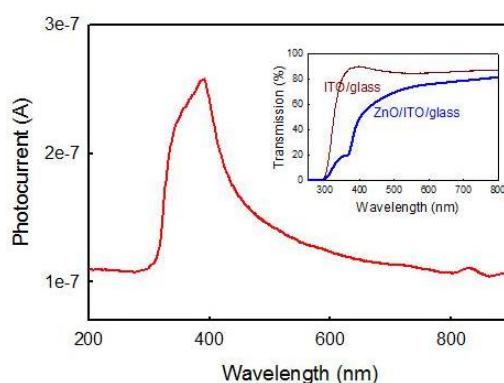


Fig. 7 Spectral photocurrent response of a device biased at 5 V. The inset shows the absorption spectra of ITO/glass and ZnO/ITO/glass structures.

3. Conclusions

A ZnO/PbS QD heterojunction was fabricated through solution processing, and its photoconductive behaviors were investigated. The devices exhibited an ultralow dark current of 10^{-12} A at a 5 V bias. Under illumination by a 70 W/m^2 incandescent lamp, a photocurrent on/off ratio greater than 10^4 was obtained. A comparative study of single-layer structures confirms that the photocurrent response originates from exciton dissociation at the depleted heterojunction. The devices, however, exhibited low responsivity of 0.02 A/W and peak quantum efficiency of 0.3%, mainly due to poor charge transport through the solution-processed ZnO and QD layers.

Reference Cited

1. D. V. Talapin, J. Lee, M. V. Kovalenko and E. V. Shevchenko, *Chem. Rev.* 110, 389 (2010).
2. R. Acharya, Y. Q. Zhang, and X. A. Cao, *Thin Solid Films*, 520, 6130 (2012).
3. O. Katz, G. Bahir, J. Salzman, *Appl. Phys. Lett.* 84, 4092 (2004).
4. Y. Q. Zhang and X. A. Cao, *Nanotechnology*, 23, 275702 (2012).
5. Y. Sun, J. H. Seo, C. J. Takacs, J. Seifert, A. J. Heeger, *Adv. Mater.* 23 (14), 1679–1683, 2011.
6. J. Tang, K. Kemp, S. Hoogland, K. S. Jeong, H. Liu, L. Levina, M. Furukawa, X. Wang, R. Debnath, D. Cha, K. Chou, A. Fischer, A. Amassian, J. B. Asbury, and E. H. Sargent, *Nature Materials*, 10, 765-771 (2011).

REPORT OF INVENTIONS AND SUBCONTRACTS
(Pursuant to "Patent Rights" Contract Clause) (See Instructions on back)

The public reporting burden for this collection of information is estimated to average 1 hour per response, including the time for reviewing instructions, searching existing data sources, gathering and maintaining the data needed, and completing and reviewing the collection of information. Send comments regarding this burden estimate or any other aspect of this collection of information, including suggestions for reducing the burden, to the Department of Defense, Executive Services Directorate (9000-0095). Respondents should be aware that notwithstanding any other provision of law, no person shall be subject to any penalty for failing to comply with a collection of information if it does not display a currently valid OMB control number.

PLEASE DO NOT RETURN YOUR COMPLETED FORM TO THE ABOVE ORGANIZATION. RETURN COMPLETED FORM TO THE CONTRACTING OFFICER.

1.a. NAME OF CONTRACTOR/SUBCONTRACTOR West Virginia University Research Corp	2.a. NAME OF GOVERNMENT PRIME CONTRACTOR U.S. Army Research Office	3. TYPE OF REPORT (X one) a. INTERIM <input type="checkbox"/> b. FINAL <input checked="" type="checkbox"/>
b. ADDRESS (Include ZIP Code) 886 Chestnut Ridge Road/PO Box 6845 Morgantown, WV 26506-6845	d. AWARD DATE (YYYYMMDD) 20140609	4. REPORTING PERIOD (YYYYMMDD) a. FROM 20140901 b. TO 20150531

SECTION I - SUBJECT INVENTIONS

5. "SUBJECT INVENTIONS" REQUIRED TO BE REPORTED BY CONTRACTOR/SUBCONTRACTOR (If "None," so state)		ELECTION TO FILE PATENT APPLICATIONS (X)		CONFIRMATORY INSTRUMENT OR ASSIGNMENT FORWARDED TO CONTRACTING OFFICER (X)	
NAME(S) OF INVENTOR(S) (Last, First, Middle Initial)	TITLE OF INVENTION(S) b.	DISCLOSURE NUMBER, PATENT APPLICATION SERIAL NUMBER OR PATENT NUMBER c.		E.	
		(1) UNITED STATES	(2) FOREIGN	(a) YES	(b) NO
None					
f. EMPLOYER OF INVENTOR(S) NOT EMPLOYED BY CONTRACTOR/SUBCONTRACTOR	g. ELECTED FOREIGN COUNTRIES IN WHICH A PATENT APPLICATION WILL BE FILED				
(1) (a) NAME OF INVENTOR (Last, First, Middle Initial)	(1) TITLE OF INVENTION	(2) FOREIGN COUNTRIES OF PATENT APPLICATION			
(b) NAME OF EMPLOYER					
(c) ADDRESS OF EMPLOYER (Include ZIP Code)					

SECTION II - SUBCONTRACTS (Containing a "Patent Rights" clause)

6. SUBCONTRACTS AWARDED BY CONTRACTOR/SUBCONTRACTOR (If "None," so state)		FAR "PATENT RIGHTS" d.		SUBCONTRACT DATES (YYYYMMDD)	
NAME OF SUBCONTRACTOR(S) a.	ADDRESS (Include ZIP Code) b.	SUBCONTRACT NUMBER(S) c.	(1) CLAUSE NUMBER	(2) DATE (YYYYMM)	DESCRIPTION OF WORK TO BE PERFORMED UNDER SUBCONTRACT(S) e.
None					

SECTION III - CERTIFICATION

7. CERTIFICATION OF REPORT BY CONTRACTOR/SUBCONTRACTOR (Not required if: (X as appropriate))	<input checked="" type="checkbox"/> SMALL BUSINESS or	<input checked="" type="checkbox"/> NONPROFIT ORGANIZATION
I certify that the reporting party has procedures for prompt identification and timely disclosure of "Subject Inventions," that such procedures have been followed and that all "Subject Inventions" have been reported.		
a. NAME OF AUTHORIZED CONTRACTOR/SUBCONTRACTOR OFFICIAL (Last, First, Middle Initial) Buckland, Mary Jane	b. TITLE Assistant Secretary	c. SIGNATURE 
		d. DATE SIGNED 20150827

Luminescence enhancement of nanocrystal quantum wells by bandgap and strain engineering

Xian-An Cao* and Yifei Lu

West Virginia University, Department of Computer Science and Electrical Engineering,
Morgantown, West Virginia 26506, United States

1 Abstract. CdSe-based nanocrystal quantum wells (QWs) were synthesized around CdS nano-
2 crystal quantum dots and were bandgap- and strain-engineered to achieve high-efficiency short-
wavelength luminescence. Tuning the CdSe QW width in the range of 1.05 to 1.58 nm has led to
blue-green light emission, whose quantum yield was improved up to 48% through strain compen-
sation by an optimized ZnS outer shell. The luminescence spectrum can be modified by adding a
ZnS inner barrier layer to block charge and exciton transfer between the QW and CdS core.
Strain management by adjusting the well and barrier thickness has proven critical in such a
complex multilayer quantum system for obtaining high-quality nanocrystals and light emission.
© 2015 Society of Photo-Optical Instrumentation Engineers (SPIE) [DOI: [10.1117/1.JNP.9.XXXXXX](https://doi.org/10.1117/1.JNP.9.XXXXXX)]

Keywords: nanocrystal; photoluminescence; quantum dot; quantum well; transmission.

Paper 15046 received Jun. 9, 2015; accepted for publication Aug. 14, 2015.

1 Introduction

Nanocrystal quantum well (NQW) is a unique type of nanocrystal heterostructure, which can be synthesized by a low-cost colloidal chemical process.^{1,2} A typical NQW, also called quantum dot (QD)-QW, consists of a core QD of a large bandgap material surrounded by an intermediate shell of a smaller bandgap material and an outer shell of the same large bandgap material as the core.³⁻⁷ In analogy with a planar single QW structure produced by vacuum epitaxy techniques, the intermediate shell acts as a circular QW, whereas the core and outer shells function as two quantum barrier layers. NQWs are of high scientific and practical interest since they can be extensively bandgap-engineered to achieve ideal properties and performance enhancement. The QW width can be tailored independent of the overall nanocrystal size to obtain a desirable optical wavelength. This adds to the already excellent tunability of colloidal nanocrystals through size and composition variations, allowing multifaceted tuning of the optical and electronic properties of nanoparticles based on a single material system.¹ On the other hand, strain buildup in such multilayer nanocrystals due to lattice mismatches would have a significant impact on the crystal quality and should be carefully managed.² However, little research effort has been devoted to strain engineering in such a nanocrystal heterostructure. As luminophores, two-dimensional NQWs have advantages over simple zero-dimensional QDs because they have a larger cross-section, which enables more efficient energy transfer and charge injection, giving rise to more efficient luminescence.

Relatively bright red, yellow, and green light-emitting diodes have been realized based on colloidal CdSe QDs with various dot sizes.⁸⁻¹¹ In principle, pure blue light emission desirable for flat-panel displays can be obtained from small CdSe QDs on the order of 1.5 nm. However, synthesis of such small QDs with a narrow size distribution and a high quantum efficiency requires a strict control of the process condition and is, thus, very challenging.¹² Overgrowth of a uniform passivating shell on top of such small QDs is also difficult. In addition, the small absorption cross-sections of the tiny QDs would limit the rate of excitonic energy transfer and charge injection. All these factors make CdSe QDs a poor choice for achieving efficient blue luminescence. To date, CdSe QDs emitting bright blue light remain elusive, and high-efficiency pure blue

*Address all correspondence to: Xian-An Cao, E-mail: xacao@mail.wvu.edu

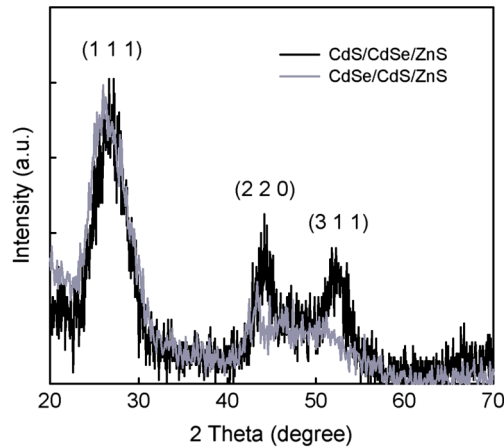


Fig. 1 X-ray diffraction patterns of CdS/CdSe/ZnS and CdSe/CdS/ZnS nanocrystals.

emission has only been obtained from interfused CdSe//ZnS nanocrystals.¹³ As discussed above, the concept of NQW provides an alternative way to obtain blue luminescence from CdSe. A narrow CdSe QW can be incorporated into relatively large nanocrystals with ease using the existing colloidal synthesis technique. This would open up a pathway toward low-cost full-color displays based on the single CdSe material system.

In a recent study, we demonstrated blue photoluminescence (PL) and electroluminescence (EL) from an asymmetrical CdS/CdSe/ZnS NQW structure.¹⁴ Both CdS and ZnS have a smaller lattice constant than CdSe, and their lattice mismatches with CdSe are 3.7 and 12%, respectively. Therefore, CdS provides a more desirable template for coherent growth of the CdSe QW, whereas ZnS provides a more effective passivation and carrier confinement due to its wider bandgap. As a result, the asymmetrical NQWs would enjoy the combined benefits of low strain in symmetrical CdS/CdSe/CdS NQWs and strong quantum confinement in symmetrical ZnS/CdSe/ZnS NQWs. Another advantage of the CdS/CdSe/ZnS NQW structure is that it is strain-compensated, as the tensile-stressed ZnS outer shell partially compensates the compressive strain in the CdSe QW layer. The nanocrystal quality is thus improved. This effect has been verified by a comparison between CdS/CdSe/ZnS and CdSe/CdS/ZnS nanocrystals, whose powder x-ray diffraction (XRD) patterns are shown in Fig. 1. Three distinct diffraction peaks corresponding to the (111), (220), and (311) crystalline planes of zinc-blende, CdS, and CdSe are seen for both samples. In the CdSe/CdS/ZnS nanocrystals, strain is not compensated as both the CdS and ZnS layers are under tensile stress, whereas the CdS/CdSe/ZnS nanocrystals are strain-compensated. As seen, the latter exhibit sharper diffraction peaks, indicating their better crystalline quality.

As a multilayer heterostructure and multiple quantum system, the CdS/CdSe/ZnS NQW provides an ideal template for engineering of nanocrystals. In this paper, we implement systematical bandgap and strain engineering of CdS/CdSe/ZnS NQWs by modifying their layer structures in an effort to achieve enhanced short-wavelength luminescence from CdSe-based nanocrystals, especially at blue-green wavelengths.

2 Experimental Details

Colloidal NQW nanocrystals with the different cross-sections shown in Fig. 2 were synthesized by the hot-injection technique. Their energy band diagrams are also illustrated, showing that both CdS and ZnS form a type I heterojunction with CdSe. All the NQWs were built atop CdS QDs synthesized using CdO and S as precursors. The size of the CdS QDs was estimated to be 3.6 nm using their absorption results and the published sizing curves.¹⁵ To synthesize CdS/CdSe/ZnS NQWs, a CdSe layer and a ZnS layer were grown in sequence around purified CdS QDs at 260°C using the successive ion layer adsorption and reaction method.¹⁶ The CdSe QW width was varied from 1 monolayer (ML) to 4.5 MLs, whereas the ZnS layer thickness was varied from 1 to 4 MLs. Given that the nanoparticles crystallize in the zinc-blende structure, each ML of CdSe and ZnS increased the nanocrystal diameter by ~ 0.7 and ~ 0.62 nm,

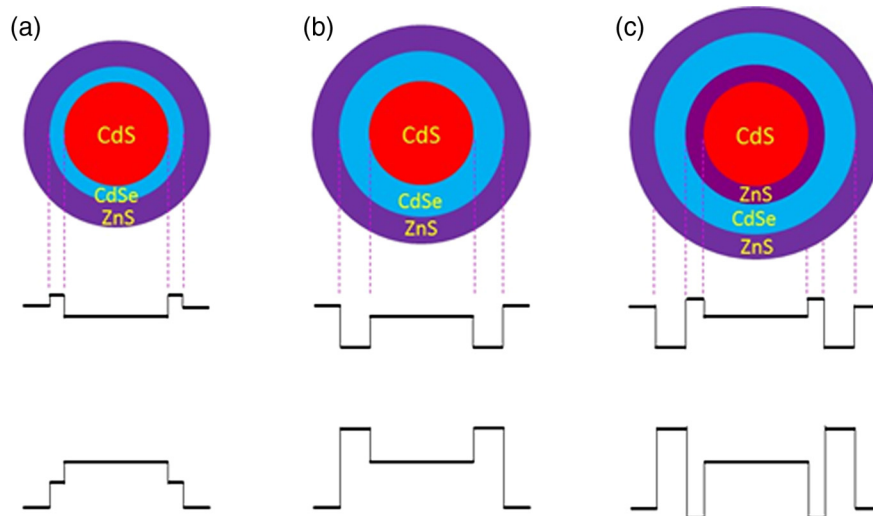


Fig. 2 Schematic cross-sections and energy band diagrams of different nanocrystal heterostructures studied in this work.

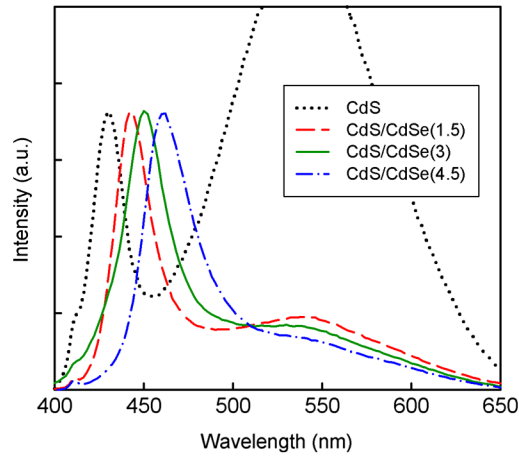


Fig. 3 Photoluminescence (PL) spectra of CdS/CdSe [0 to 4.5 monolayers (MLs)] nanocrystals. The main peak intensity was normalized.

respectively. Hence, the well width was in the range of 0.35 to 1.58 nm, and the ZnS outer shell ranged from 0.31 to 1.24 nm. In a modified NQW structure, a 2 or 2.5 ML ZnS interlayer was inserted between the CdS core and CdSe layer acting as the inner quantum barrier layer.

During the NQW synthesis, a 1 ml sample was extracted after growth of the core and each ML of the shell. The samples were washed by hexane and used for absorption and PL measurements. The absorption and PL spectra were measured using a Hitachi U-3900H double-beam UV-VIS spectrophotometer and a Hitachi F-7000 fluorescence spectrophotometer (365 nm excitation), respectively. The PL quantum yields (QYs) were estimated by comparing the PL intensity with that of standard organic dye solutions with the same optical density at the same excitation wavelength. The nanocrystal crystallinity was examined by powder XRD on a Bruker D8 Discover X-Ray Diffractometer using Cu $K\alpha$ radiation ($\lambda = 0.1542$ nm).

3 Results and Discussion

Figure 3 shows the PL spectra of CdS/CdSe (0 to 4.5 MLs) nanocrystals with a typical core/shell structure. The PL spectrum of the CdS core consists of a sharp excitonic emission peak at 430 nm and a more dominant broad band, which is centered at 540 nm and spans almost the entire visible spectrum. The broadband can be attributed to excitonic decay via surface states, which originate

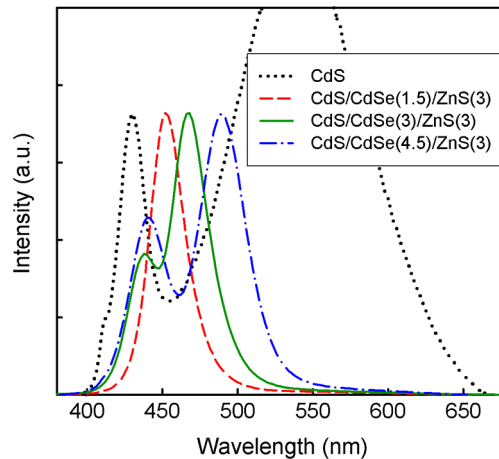


Fig. 4 PL spectra of CdS/CdSe (0 to 4.5 MLs)/ZnS (3 MLs) nanocrystals. The main peak intensity was normalized.

from surface dangling bonds and behave as effective nonradiative recombination centers.¹⁷ Upon the growth of CdSe, the main PL peak exhibits a redshift and broadening, and the surface state emission is substantially suppressed. With 1.5, 3, and 4.5 MLs of CdSe, the peak redshifts by 12, 20, and 31 nm, respectively. Since the bandgap of CdSe is a function of its layer thickness due to the quantum size effects, the initial thin CdSe shell may have a wider bandgap than the CdS core as illustrated in Fig. 2(a) and, thus, acts as a confining layer. In this case, the redshift can be attributed to penetration of the electron and hole wave functions into the CdSe layer, resulting in weaker quantum confinement. As the CdSe layer grows thicker, its bandgap shrinks and becomes narrower than the core [Fig. 2(b)]. In this case, the PL may mainly originate from the CdSe shell as excitons generated in the core can readily diffuse or transfer energy into the shell.

Figure 4 shows the PL spectra of the same nanocrystals after further overgrowth of a 3 ML ZnS outer shell. In the resulting heterostructures, the long-wavelength broadband emission is completely eliminated, confirming the excellent passivation and charge confinement by ZnS. The main peak further shifts to 451, 468, and 489 nm for the nanoparticles with 1.5, 3, and 4.5 MLs of CdSe. Another interesting feature is that a secondary peak at ~439 nm appears for the nanoparticles with 3 or 4.5 ML CdSe. This is very close to the original CdS core PL peak (430 nm). Referring to the energy band diagrams shown in Fig. 2, we can explain the origin of the secondary peak as follows. When the CdSe layer thickness reaches 3 MLs or thicker, its bandgap becomes narrower than that of the core. As a result, a well-defined CdSe QW is created with the ZnS shell and CdS core acting as two barrier layers. The main peak (at 489 nm for 4.5 ML CdSe) represents luminescence from the CdSe QW, whereas the 439 nm peak originates from the CdS core. The latter emerges due to charge overflow into the core as all states in the QW are filled under optical excitation. Without a passivating ZnS outer shell (Fig. 3), excitons in CdSe may recombine rapidly through surface states, so charge overflow would not occur. As seen, the PL spectrum of the nanocrystal with 1.5 ML CdSe remains a single peak. This suggests that the bandgap of 1.5 ML CdSe is wider than the CdS core, and the CdSe layer functions as a confining shell instead of a single QW.

The formation of a CdSe NQW is confirmed by absorption measurements. Figure 5 shows the absorption spectra of CdS/CdSe (4.5 MLs)/ZnS (3 MLs) NQWs measured after each ML shell growth. The absorption spectrum of the CdS core features the first excitonic absorption peak at 407 nm. The absorption peaks shift toward the longer wavelength as the CdSe and ZnS shells grow thicker, whereas the excitonic features remain nearly unchanged. The total redshift of the first excitonic absorption peak is 31 nm after the growth of the 4.5 MLs of CdSe, which is identical to the total PL peak shift of the same nanocrystal (Fig. 3). Upon the addition of a ZnS outer shell, the absorption behavior becomes considerably different. A prominent new feature is that short-wavelength absorption is greatly enhanced, as indicated by a sharper high-order excitonic absorption peak around 400 nm. This can be attributed to a newly emerged absorbing element in addition to the core QD, that is, a CdSe QW that can absorb light efficiently due to strong quantum confinement. These results suggest that through bandgap engineering, a

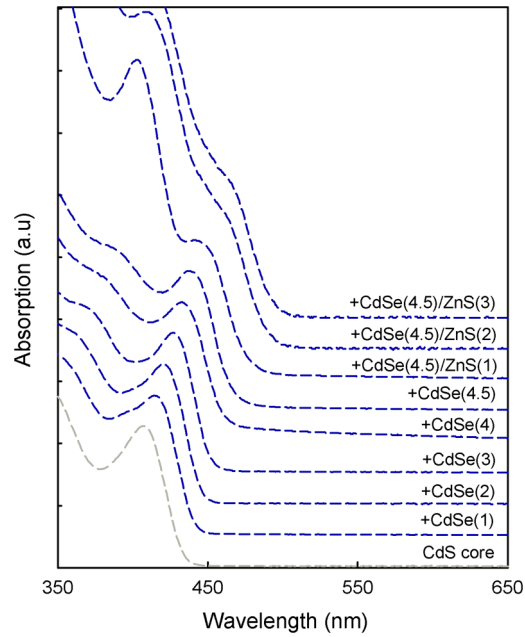


Fig. 5 Evolution of the absorption spectrum of CdS/CdSe (4.5 MLs)/ZnS (3 MLs) nanocrystal quantum wells (NQWs) during the shell growth. The spectra were normalized and shifted in the y-direction for clarity.

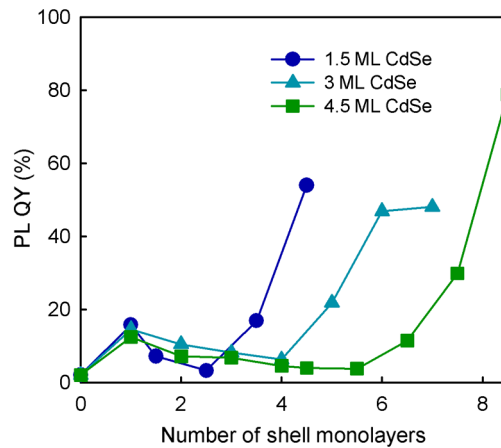


Fig. 6 PL quantum yields of three types of CdS/CdSe/ZnS NQWs measured after each ML of shell growth.

new efficient light absorbing and emitting NQW structure can be created, and the absorption and emission peaks can be tuned continuously toward the longer wavelength.

Figure 6 plots the PL QYs of the above three types of NQWs measured after the growth of each ML of the shell. All the curves are of a reverse S shape. As the shell synthesis proceeds, the QY increases, then decreases, and finally increases again. This trend reflects a trade-off between the beneficial and adverse effects of the shell overgrowth. The QY of the CdS core QDs is only ~2% due to a strong influence of surface states. The overgrowth of 1 ML CdSe raises the value to 13 to 16% as a result of surface passivation. The QY tends to decrease as the CdSe layer grows thicker than 2 MLs. This indicates strain buildup in the CdS/CdSe core/shell structure, causing deterioration of the crystal quality. The CdSe layer grown on CdS QDs is under compressive strain due to its larger lattice constant. The initial CdSe growth is coherent and the layer undergoes elastic deformation. Strain builds up as the CdSe layer grows, leading to increased nanocrystal irregularity and nonuniformity.² This partly explains the increased PL linewidth seen in Figs. 3 and 4. When a critical thickness is reached, strain is partially relieved through the

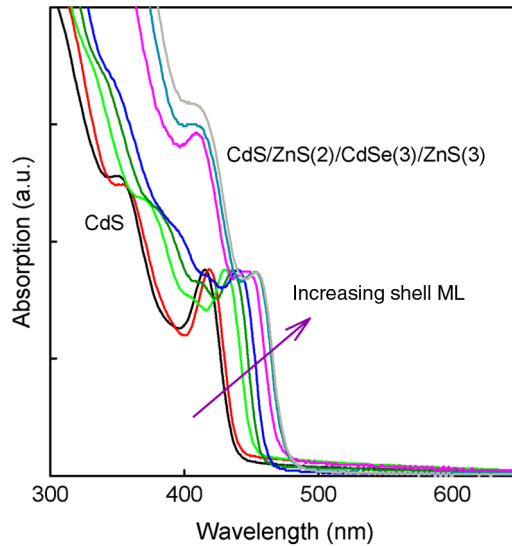


Fig. 7 Evolution of the absorption spectra of CdS/ZnS (2 MLs)/CdSe (4.5 MLs)/ZnS (3 MLs) NQWs during the shell growth.

formation of misfit dislocations at the interface,^{1,2} which act as nonradiative recombination sites and cause PL degradation. With a 4.5 ML CdSe shell, the QY drops to 4%.

As seen in Fig. 6, the PL QY is remarkably improved upon the growth of the wide bandgap ZnS outer shell, which enables more effective carrier confinement and surface passivation. Meanwhile, the ZnS shell also acts as a strain-compensation layer as it has a smaller lattice constant than CdSe.¹¹ The compressive strain in the CdSe QW is partially compensated, leading to better crystal quality. With 3 ML ZnS, the QYs of the nanocrystals with 1.5, 3, and 4.5 ML CdSe reach 30, 47, and 54%, respectively. Strain compensation appears to be particularly beneficial in NQWs with a thick QW. Upon growth of the fourth ML of ZnS, the QY of CdS/CdSe (4.5 MLs)/ZnS NQWs is further increased to 78%, whereas it is only slightly higher (48%) in the NQWs with 3 ML CdSe. For the latter, the QY reaches the saturation point and a thicker ZnS shell would cause defect generation and QY reduction. The PL QY of the QW emission can be estimated based on the spectral data, which show that the intensity of green-blue emission from the QW is ~ 1.6 times higher than that of the CdS core emission in the CdS/CdSe (4.5 MLs)/ZnS (4 MLs) NQWs. The PL QY of the CdSe QW is thus $\sim 48\%$. Similarly, the 3 ML CdSe QW emitting pure blue light at 468 nm has an estimated QY of 35%. Such high efficiencies of short-wavelength emission from CdSe nanocrystals have rarely been reported before.²

As seen from Fig. 2, one drawback of the asymmetrical NQW is that the CdS core functions as the inner barrier layer, but cannot effectively confine excitons due to relatively small band offsets at the CdS/CdSe interface. Emission from the core is inevitable under high excitation levels resulting from carrier overflow and exciton transfer from the QW. To achieve better confinement, we inserted a ZnS layer between the CdS core and CdSe QW, and the resulting structure is shown in Fig. 2(c). Figure 7 shows the absorption spectra of CdS/ZnS (2 MLs)/CdSe (3 MLs)/ZnS (3 MLs) NQWs measured after each ML shell growth. Again, the absorption peaks redshift as the shell grows. Upon the growth of the outer ZnS shell, the absorption at short wavelengths is greatly enhanced and high-order excitonic peaks become more pronounced, indicating the formation of a ZnS/CdSe/ZnS NQW. The thicknesses of the ZnS and CdSe layers are critical as they determine the amount of strain buildup and the degree of strain compensation in the whole nanocrystal structure. This can be clearly seen in Fig. 8, which compares the absorption spectra of NQWs with 2 or 3 MLs of ZnS inner barrier layer and 2.5 or 3 MLs of CdSe QW. For the NQW with a 3 ML ZnS/2.5 ML CdSe, the absorption spectrum is nearly featureless, suggesting poor crystal quality. This is caused by large tensile strain in the thick ZnS layer, which cannot be compensated by the thin CdSe overlayer. More effective strain compensation and, thus, better crystal quality is obtained by reducing the ZnS thickness and increasing the CdSe well width. As seen, the NQW with 2 ML ZnS/3 ML CdSe exhibits the sharpest excitonic absorption peaks.

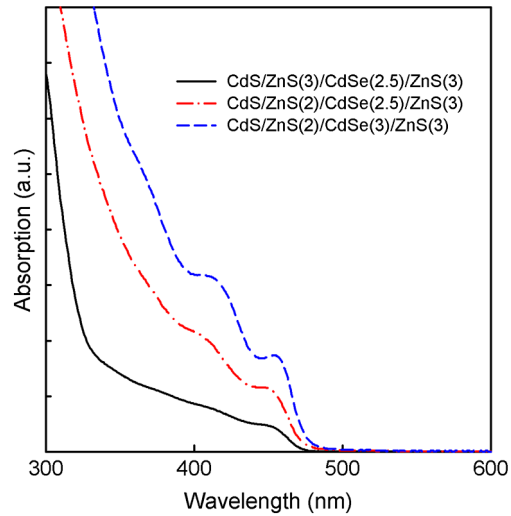


Fig. 8 Absorption spectra of CdS/ZnS (2 or 3 MLs)/CdSe (2.5 or 3 MLs)/ZnS (3 MLs) NQWs.

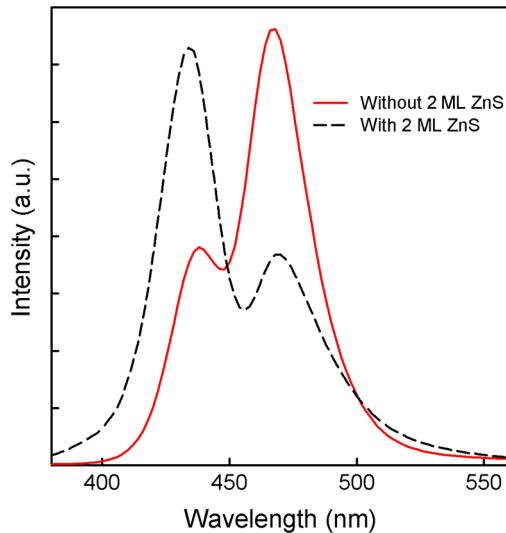


Fig. 9 PL spectra of CdS/CdSe (3 MLs)/ZnS (3 MLs) NQWs and CdS/ZnS (2 MLs)/CdSe (3 MLs)/ZnS (3 MLs) NQWs.

The PL spectra of the strain-compensated CdS/ZnS (2 MLs)/CdSe (3 MLs)/ZnS NQW is compared with that of CdS/CdSe (3 MLs)/ZnS NQWs in Fig. 9. For both NQWs, the PL spectrum is composed of the QW emission at ~ 468 nm and the core emission near 435 nm. However, the intensity ratios of these two peaks are different. The ratio is changed from 2 : 1 to roughly 1 : 2 after the addition of the 2 ML inner ZnS layer. This result actually confirms the effective blocking of carriers and excitons by the additional ZnS layer. Under optical excitation, excitons can be generated in both the CdS core and CdSe QW. As the transfer of charge and excitons from the core to the QW is blocked, the relative intensity of the core emission increases. We can expect that the core emission would be absent from a light-emitting device with such NQWs incorporated as the luminophores because excitons cannot be directly created in the CdS core under current injection. Therefore, EL comprising pure QW emission is expected. Further work will focus on the design and demonstration of such a device in order to verify this assumption.

4 Conclusions

In summary, colloidal CdS/CdSe/ZnS NQW nanocrystals were bandgap- and strain-engineered to achieve efficient luminescence at short wavelengths. Blue and green light emission has been

achieved by tuning the CdSe QW width in the range of 3 to 4.5 MLs, and enhanced through strain management. It has been found that for a wider QW, a thicker ZnS outer shell is needed for effective confinement as well as strain compensation, which led to blue-green luminescence peaking at 489 nm with a QY of ~48%. The charge and exciton transfer between the QW and CdS core was effectively blocked by adding a ZnS inner barrier layer. Strain engineering by tailoring the thicknesses of the QW and barrier layers has proven critical for obtaining high nanocrystal quality and superior optical properties.

Acknowledgments

This work was supported in part by a grant from the Army Research Office, No. W911NF-14-1-0292, monitored by Dr. William W. Clark.

References

1. P. Reiss, M. Protière, and L. Li, "Core/shell semiconductor nanocrystals," *Small* **5**(2), 154–168 (2009).
2. D. V. Talapin et al., "Prospects of colloidal nanocrystals for electronic and optoelectronic applications," *Chem. Rev.* **110**(1), 389–458 (2010).
3. M. Braun, C. Burda, and M. A. El-Sayed, "Variation of the thickness and number of wells in the CdS/HgS/CdS quantum dot quantum well system," *J. Phys. Chem.* **105**, 5548–5551 (2001).
4. Z. Xu et al., "InGaAs/GaAs quantum-dot-quantum-well heterostructure formed by submonolayer deposition," *Nanotechnology*. **14**, 1259 (2003).
5. A. W. Schill et al., "Ultrafast electronic relaxation and charge-carrier localization in CdS/CdSe/CdS quantum-dot quantum-well heterostructures," *Nano Lett.* **6**, 1940–1949 (2006).
6. S. Nizamoglu and H. V. Demir, "Onion-like (CdSe) ZnS/CdSe/ZnS quantum-dot-quantum-well heteronanocrystals for investigation of multi-color emission," *Opt. Express* **16**, 3515–3526 (2008).
7. R. Kostić and D. Stojanović, "Influence of the internal heterostructure on nonlinear refractive index changes for intersubband transitions in spherical quantum dot quantum well nanoparticles," *J. Nanophoton.* **6**(1), 061604 (2012).
8. Y. Shirasaki et al., "Emergence of colloidal quantum-dot light-emitting technologies," *Nat. Photonics* **7**, 13–23 (2013).
9. W. K. Bae et al., "Multicolored light-emitting diodes based on all-quantum-dot multilayer films using layer-by-layer assembly method," *Nano Lett.* **10**, 2368–2373 (2010).
10. Y. Q. Zhang and X. A. Cao, "Electroluminescence of green CdSe/ZnS quantum dots enhanced by harvesting excitons from phosphorescent molecules," *Appl. Phys. Lett.* **97**, 253115 (2010).
11. Y. Lu, Y. Q. Zhang, and X. A. Cao, "Improved luminescence from CdSe quantum dots with a strain-compensated shell," *Appl. Phys. Lett.* **102**, 023106 (2013).
12. A. Rizzo et al., "Blue light emitting diodes based on fluorescent CdSe/ZnS nanocrystals," *Appl. Phys. Lett.* **90**, 051106 (2007).
- 6 13. S. Jun and E. Jang, "Interfused semiconductor nanocrystals: brilliant blue photoluminescence and electroluminescence," *Chem. Commun.* 4616–4618 (2005).
14. Y. Lu, Y. Q. Zhang, and X. A. Cao, "Blue and green electroluminescence from CdSe nanocrystal quantum-dot-quantum-wells," *Appl. Phys. Lett.* **105**, 203101 (2014).
15. W. W. Yu et al., "Experimental determination of the extinction coefficient of CdTe, CdSe, and CdS nanocrystals," *Chem. Mater.* **15**, 2854–2860 (2003).
16. J. J. Li et al., "Large-scale synthesis of nearly monodisperse CdSe/CdS core/shell nanocrystals using air-stable reagents via successive ion layer adsorption and reaction," *J. Am. Chem. Soc.* **125**, 12567–12575 (2003).
17. J. S. Steckel et al., "Blue luminescence from (CdS)ZnS core-shell nanocrystals," *Angew. Chem. Int. Ed.* **43**, 2154–2158 (2004).

7 Biographies for the authors are not available.